Received: April 18, 2023. Revised: July 13, 2023.

INASS

International Journal of
Intelligent Engineering & Systems

http://www.inass.org/

Light Field Hyper Spectral Lossless Compression Employing Greedy Discrete Wavelet and Poincare Recurrence Network

Anjaneya P[1] **Rajini G. K[1]***

[1]*School of Electronics Engineering, Vellore Institute of Technology, Vellore, Tamilnadu, India*
* Corresponding author's Email: rajini.gk@vit.ac.in

Abstract: Light field imaging, which can gather global visual data, has garnered attention from the computer world in recent years. Inter and intra frame correlation, big data storage, and poor reconstructed depth quality still plague light field area. In this work, greedy discrete wavelet and poincare recurrence network (GDW-PRN) is proposed for robust lossless image compression of hyper spectral images. First, spatial preprocessing is carried out using discrete reduction wavelet transform to remove unwanted artifacts. Next, dimensionality reduced visual data representation is applied by means of greedy band to the pre-processed images, therefore addressing the issues related to large data storage. Finally, lossless image compression is performed by utilizing poincare recurrence network. The entire proposed work was carried out on light field hyperspectral imagery data using MATLAB simulation tool. The proposed work has been compared to the existing methods such as compression based on differential pulse code modulation (C-DPCM), and 3D wavelet transform and spectrum learning with regression vector (3DWT-SRV). On comparison the acquired findings demonstrate that the suggested GDW-PRN process has high compression proportion light field image storage performance as well as leading to high peak signal to noise ratio (PSNR).

Keywords: Light field image, Lossless compression, Discrete reduction wavelet, Spatial preprocessing, Greedy band, Poincare recurrence, Neural network.

1. Introduction

Military, crop, and marine pollution monitoring use hyperspectral remote sensing. The top space agencies in the world have grouped together to form a consortium called the consultative committee for space data systems (CCSDS). Several widely used lossless compression methods have been suggested for hyperspectral imagery. Using differential-pulse-code-modulation, a deep learning method for lossless compression in hyperspectral images, improves PSNR and prediction accuracy [1]. Spectral information pitfalls improved prediction accuracy but decreased PSNR. Affinity between adjacent bands will design a discrete reduction wavelet transform spatial preprocessing and greedy band dimensionality. Maximizing correlation and compressing reduces visual data representation.

Based on 3D coefficient regression, 3D wavelet transform and spectrum learning with regression vector (3DWT-SRV) was proposed in [2]. HSIs were sparsely represented using a 3D wavelet transform. The peak signal-to-noise ratio (PSNR) and the accuracy of classification were the primary research objectives, while compression ratio was ignored. Poincare recurrence network lossless compression, using poincare recurrence theorem, improves PSNR and reduces MSE. Thus, compression proportion improves.

1.1 Contribution

The contributions of this work begin with the proposal of a novel preprocessing and dimensionality reduction method for lossless hyper spectral image compression. Secondly, the preprocessing is carried out using discrete reduction wavelet transform to remove noise. Later greedy band visual data representation is used which improves PSNR for robust dimensionality reduced hyper spectral images and also carried weight-

updating poincare recurrence network lossless image compression/decompression reduces light field image storage. Finally the the proposal is compared to existing methods on a large test bed using hyper spectral images to prove its superiority.

1.2 Paper formulation

The organized preparation of the article is presented as, section 2 evaluates the associated works done in the field of lossless image compression with light field imaging. Section 3 designates the details of the suggested greedy discrete wavelet and poincare recurrence network method. In section 4, experimental evaluation and discussion made with two standard methods is presented. Section 5 explains conclusions of the paper.

2. Related works

Light field imaging has gained attention from all walks of life, enabling a wide range of computer applications. [3] assessed light field image quality using log Gabor features to improve visual system perception. [4] covered light field imaging and its uses in compression, editing, and processing. Machine learning can compress images in lossless pattern. [5] proposed a deep residual network with meyer hat wavelet transform to compress faster.

Image compression's main drawback is storage and time. Therefore, a distributed, improved post-transform improved compression values by enhancing bit plane encoding [6-7]. The authors in [8] created a rate control algorithm to simplify and improve image compression. The authors in [9] reviewed data compression methods whereas the authors in [10] suggested deep neural networks compress images and videos. The researchers of [11] designed efficient data compression algorithms with optimal compression rate-latency trade-off. The researchers of [12] reviewed data compression methods to reduce communication data size whereas the authors of [13] suggested studying correlation factor-based image compression algorithms.

The researchers in [14] used singular value decomposition and matrix completion to retrieve and compress images efficiently (SVD). A significant limitation of SVD is that it can be computationally costly for large matrices, making it impractical for use with very large images. Additionally, SVD may not be appropriate for images with highly localised or complex structures, as the low-rank approximation generated by SVD may not accurately represent these structures. In [15] the authors presented a deep recurrent neural network for the lossless compression of multispectral and hyperspectral data. In order to accurately model the data distribution, this method requires a large amount of training data, which can be difficult to acquire for hyperspectral and multispectral data due to their high dimensionality and complexity. Moreover, training deep RNNs can be computationally costly and may necessitate specialised hardware to accomplish reasonable training times. In [16], lossless compression and pre-quantization were used to rebuild the image using convolutional neural network (CNN). Pre-quantization can result in information loss, which can affect the image's fidelity after reconstruction. This loss of information can be minimised by employing higher quantization levels, but at the expense of an increase in compression artefacts and a decrease in image quality.

Moreover, the quality of the compressed data used to train the CNN has a significant impact on the quality of the reconstructed image. If the compressed data is of poor quality or contains significant artefacts, the reconstructed image may contain these artefacts and be of lower quality. Whereas compressing medical images were presented in [17] using wavelet based volumetric medical image compression. A limitation of wavelet-based compression is that it can result in information loss, particularly when lossy compression techniques are employed. While a certain amount of loss is generally acceptable for medical images, excessive loss can lead to diminished diagnostic accuracy and misinterpretation.

In addition, the compression efficacy of wavelet-based techniques can be sensitive to the selection of wavelet basis and compression parameters, which can be difficult to optimise for various medical image types and applications. In [18], time series-based temporal correlations improved data fidelity and size. Using temporal correlations between adjacent spectral bands can minimise data storage and transmission while maintaining image quality. This approach has limitations.

Calculating temporal correlations between adjacent spectral bands is computationally expensive in time-series-based hyperspectral image compression. For big hyperspectral datasets, this slows and complicates compression.

Noise and temporal correlations can also impair image quality. Significant temporal connections between spectral bands diminish compression efficiency and reconstruction quality.

The authors in [19] presented a distributed source coding-based lossless compression algorithm.

The effectiveness of DSC-based compression can be dependent on the characteristics of the hyperspectral data that is being compressed. If spectral bands are highly correlated, DSC-based compression may not result in significant compression efficiency gains. A hybrid prediction method [20] used fractal function to reduce decoding quality and increase PSNR rate. It may be computationally challenging to derive the fractal functions used for prediction, which is a limitation of this method. Larger datasets may necessitate a lengthier computation time, which may make this method impractical for some applications.

The effectiveness of this method can also be contingent on the specific characteristics of the compressed hyperspectral data. If the spectral bands have high variability or low correlation, the accuracy of the fractal function predictions may be limited, which can result in diminished compression efficiency and lower quality reconstructions.

There have been numerous proposals for compressing hyperspectral and multispectral images, but each of the approaches described in this section has its own limitations. SVD can be computationally expensive and may not represent complex structures accurately. Deep RNNs require a significant quantity of training data and can be computationally costly. CNN pre-quantization can result in data loss and degraded image quality. Information loss is possible with wavelet-based compression, which is also sensitive to the selection of wavelet basis and compression parameters. Noise and temporal correlations can degrade time-series-based compression, which is computationally costly. The effectiveness of DSC-based compression is dependent on the characteristics of the hyperspectral data, and the hybrid prediction method may be computationally difficult for larger datasets and constrained by low correlation or high variability of spectral bands.

Based on these limitations, this paper presents a greedy discrete wavelet and poincare recurrence network (GDW-PRN) for lossless image compression of hyper spectral images to reduce light field imaging storage and improve PSNR.

3. Greedy discrete wavelet and poincare recurrence network

Light field imaging can capture more visual data than traditional photography, which can only capture a 2D representation of the light integrating angular domain.

We preprocess the hyperspectral image with discrete reduction wavelet transform to extract spatial information. In a semi-supervised graph-based framework for lossless image compression, greedy band affinity (GBA) fuses preprocessed spatial and spectral information. Finally, poincare recurrence neural network improves PSNR and provides lossless image compression. Fig. 1 shows the greedy discrete wavelet and poincare recurrence network method block diagram. Hyper spectral image lossless compression involves three steps, as shown above namely preprocessing, dimensionality reduction, and compression/decompression.

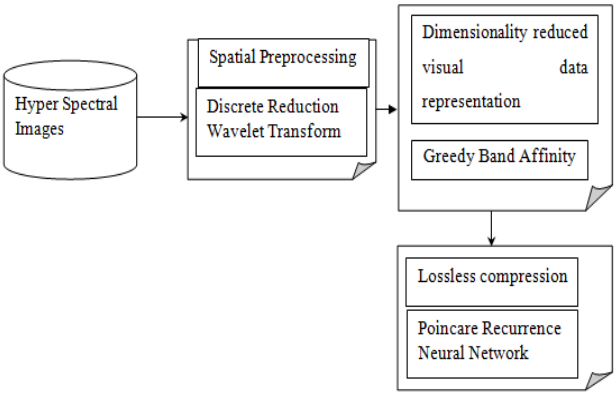

Figure. 1 Block diagram of greedy discrete wavelet and poincare recurrence network

3.1 System model

Using the hyperspectral image, a graph-based model is created. The vertices represent the input sample images, and the edges represent hyperspectral image pixel similarity. Our hyperspectral image is a graph ‘G=(V, E)', where ‘V' is the vertices set and ‘E' is the edge set.

3.2 Discrete reduction wavelet transform spatial preprocessing

To remove noise and smooth hyperspectral images, discrete reduction wavelet transform spatial preprocessing is applied. It enhances spatial texture data to advance lossless image compression. Spatial preprocessing uses discrete reduction wavelet transform. Fig. 2 illustrates discrete reduction wavelet transform spatial preprocessing.

As illustrated in the above figure, let us consider an input signal ‘ p ’ with the discrete wavelet transform measured via a filter series. Initially, it is passed via a low pass filter ‘l’ and then via a high pass filter ‘h’. This is arithmetically expressed as follows:

$$q_{low}[n] = \sum_{i=-\infty}^{\infty} p[i]l[2n-i] \quad (1)$$

$$q_{high}[n] = \sum_{i=-\infty}^{\infty} p[i]h[2n-i] \quad (2)$$

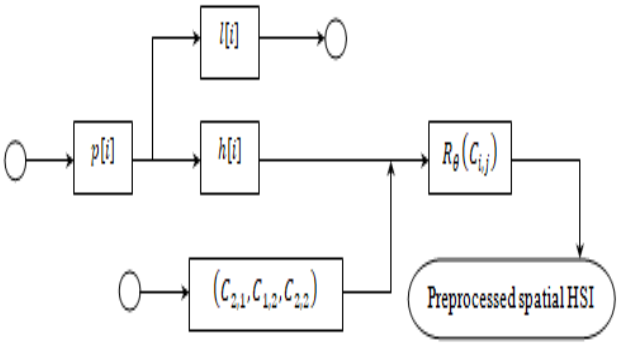

Figure. 2 Structure of discrete reduction wavelet transform spatial

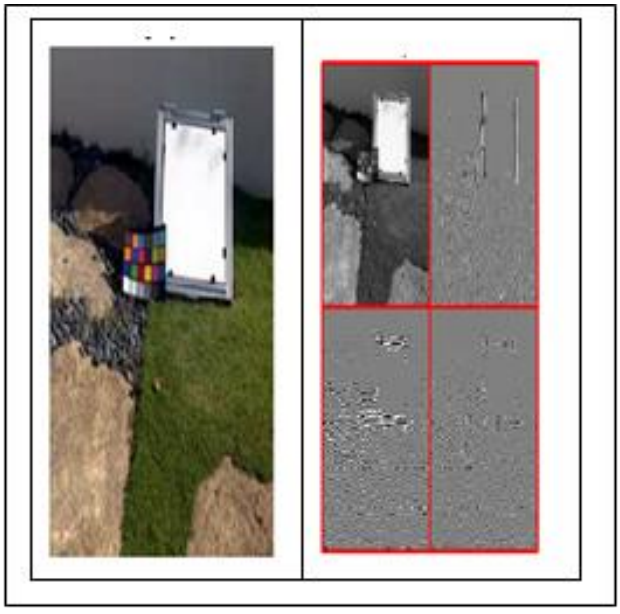

(a) (b)

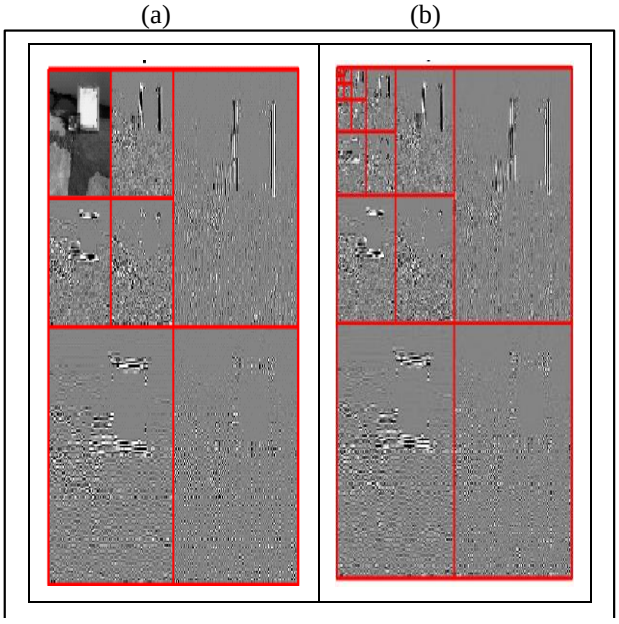

(c) (d)

Figure. 3 Discrete isotropic reduction wavelet transform: (a) Input Image, (b) Pre-Processed Image, (c) 1 * 2 band image, and (d) 2 * 2 band image

From the above two Eqs. (1) and (2), '$q_{low}[n]$', '$q_{high}[n]$' represents the resultant low pass and high pass filter for the corresponding input signal 'p' sub sampled by '2', further processing with high pass 'h' and low pass 'l' filter, x represents multiplication and is written simply as given below.

$$q_{low} = (p\ x\ l) \downarrow 2 \tag{3}$$

$$q_{high} = (p\ x\ h) \downarrow 2 \tag{4}$$

From the above Eqs. (3) and (4), 'q_{low}' and 'q_{high}', forms the new low pass filter and high pass filter correspondingly. Our spatial preprocessing uses discrete isotropic reduction wavelet transform with these filter values. Coefficient 'C (i,j)' orthogonalizes signal 'p'. This is further applied to high pass coefficients using wavelet reduction function '$R_\theta(C_{i,j})$' and '$\alpha(C) = \left\{c_{21}^{1/2}, c_{12}^{1/2}, c_{22}^{1/2}\right\}$'. This is mathematically formulated as given below.

$$R_\theta(C_{i,j}) = \begin{cases} C_{i,j} - \frac{\theta}{\alpha(C)}, if\, \alpha(C) \geq \theta \\ 0, Otherwise \end{cases} \tag{5}$$

Fig. 3 given below shows the resultant discrete isotropic reduction wavelet transform spatial preprocessed image when applied to the input signal.

Fig. 3 given above shows the original input HIS. Next, pre-processed image in the range of 2 * 1 band images is shown in (b), a 1 * 2 band image is shown in (c) and 2 * 2 band images is depicted in (d) via wavelet reduction function.

3.3 Greedy band dimensionality reduced visual data representation

After wavelet reduction, greedy band affinity is applied to each band of the hyper spectral preprocessed highly correlated image. In our paper, greedy band ordering minimises the dimensionality of preprocessed HIS data in affine "A" direction, which includes a number of interrelated signals, while retaining divergences via correlation. The affinity between bands for a distortion increases.

The measured value that discloses the proximity between the two independent bands is the spectral band correlation. It represents the affinity between the two bands 'b_i' and 'b_j' indicated as a coefficient expressed as given below.

$$DRI = A_{b_1 b_2} = \frac{\sum_{i=1}^{m}\sum_{j=1}^{n}[b_1(i,j)]-[b_2(i,j)]}{\sqrt{\sum_{i=1}^{m}\sum_{j=1}^{n}[b_1(i,j)]^2}\sqrt{\sum_{i=1}^{m}\sum_{j=1}^{n}[b_2(i,j)]^2}} \tag{6}$$

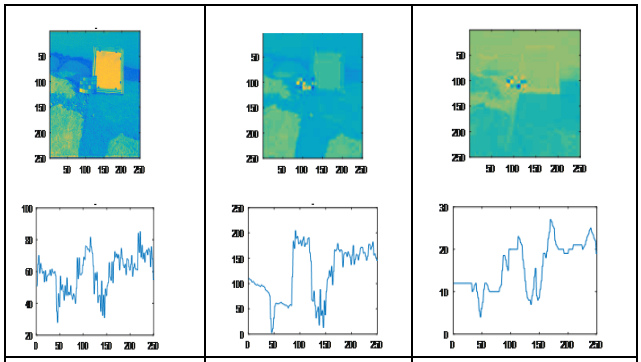

Dimensionality Variation 1	**Dimensionality Variation 2**	**Dimensionality Variation 3**

(a) (b) (c)

Figure. 4 Dimensionality reduced data representation: (a) 2 * 1 band image, (b) 1 * 2 band image, and (c) 2 * 2 band image

According to Eq. (6), bands "b 1" and "b 2" are highly affined "A" if the coefficient is high, and less affined if the coefficient is low. Dimensionality-reduced data representation with affine greedy band yields Fig. 4.

Affine proximity greedy band produces dimensionality reduced images for three bands, as shown above. Discrete reduction wavelet transform and greedy band decomposition pseudo code is below.

Algorithm 1 Discrete reduction wavelet transform and greedy band decomposition

Input: Samples '$S = s_1, s_2, \dots, s_n$'
Output: Dimensionality reduced images '$DRI = d_1, d_2, \dots., d_n$'
Step 1: **Initialize** bands 'b_1' and 'b_2' Step 2: **Begin** Step 3: **For** each samples 'S' Step 4: Evaluate discrete wavelet transform measured via filter series using equation (1) and (2) Step 5: Evaluate low and high pass filter using equation (3) and (4) Step 6: Measure wavelet reduction function using equation (5) Step 7: Obtain affinity between the two bands 'b_i' and 'b_j' using equation (6) Step 8: **Return** (dimensionality reduced images) Step 9: **End for** Step 10: **End**

3.4 Discrete reduction wavelet transform and greedy band decomposition

Discrete reduction wavelet transform and greedy band decomposition describe two processes. Dimensionality reduction, HIS preprocessing.

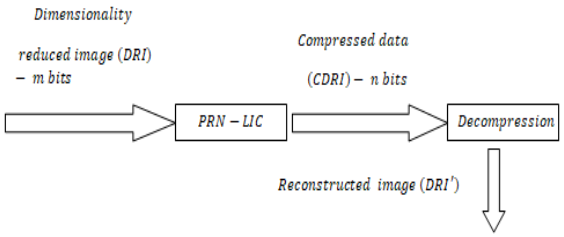

Figure. 5 Structure of poincare recurrence network lossless compression and decompression

Discrete reduction wavelet transform preprocesses high pass coefficient. Greedy band affinity dimensionality lowers wavelet. Greedy band affinity reorders bands in a preprocessed highly correlated image set to maximise band affinity and compression.

3.5 Poincare recurrence network lossless image compression

HSI is more popular for remote sensing. HSI data volume grows rapidly as spectral resolution increases, requiring a lot of storage. Lossless compression preserves image data well with a low compression ratio. Poincare recurrence network lossless image compression (PRN-LIC) improves peak signal-to-noise ratio and light field image storage. Fig. 5 illustrates poincare recurrence network lossless image compression.

As shown above, the dimensionality reduced images "DRI" are split into bands "n" of "n*n" size to reduce run time. Each band is reconstructed into an m-dimensional vector, written as 'V={v 1,v 2,...,v m }', where 'm' is the vector size. Encryption is below. First, dimensionality-reduced image is split into bands 'b_i, b_j' and weights 'W_{ij}' are generated randomly 'Rand'. The math is below.

$$W_{ij} = \left[Rand\left(b_i, b_j\right)\right] \quad (7)$$

With the aid of the weight, the hidden layer 'H_{ij}' and output layer 'O_{ij}' is measured as given below.

$$H_{ij} = \frac{1}{1+exp^{W_{ij}*V_i}} \quad (8)$$

$$O_{ij} = \frac{1}{1+exp^{V_i*H_{ij}}} \quad (9)$$

The exponential product of weight "W_{ij}" and its vector "V_i" of "m" dimension evaluates the hidden layer from Eqs. (8) and (9). The hidden layer output 'H_{ij}' and the output layer vector 'V i' of 'm' dimension are evaluated similarly. After that, the weights are updated.

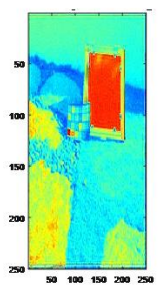
(a)

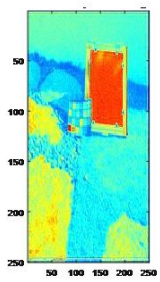
(b)

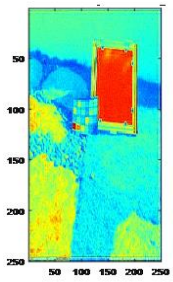
(c)

Lossless Compressed Image	**Dimensionality Reduced Image**	**Lossless De-compressed Image**

Figure. 6: (a) dimensionality reduced image, (b) lossless compressed image, and (c) lossless de-compressed image

$$\Delta W_{ij}(p) = \mu\, O_{ij}(p)\, \delta_{ij}(p) \quad (10)$$

From the above Eq. (10), the updated weights 'ΔW_{ij}' of perceptron 'p' is obtained based on the output layer resultant value '$O_{ij}(p)$', a learning factor 'μ' and error gradients '$\delta_{ij}(p)$'. The error gradient is measured as given below.

$$\delta_{ij}(p) = O_{ij}(p)\big[1 - O_{ij}(p)\big][O_D - O_A] \quad (11)$$

From the above equation (11), the error gradient for each perceptron '$\delta_{ij}(p)$' is evaluated by measuring the difference between the desired values 'O_D' and the actual value 'O_A' respectively in addition to the output layer resultant value '$O_{ij}(p)$'. Our work uses poincare recurrence (PR) to permute after error gradient measure and keep pixel values unchanged. See below.

$$T^k(b_i, b_j) = T^{k-1}\big[mode\,(2b_i + b_j, N), mod\,(b_i + b_j, N)\big] \quad (12)$$

From the above Eq. (12), 'N' corresponds to the number of pixels, with bands representing 'b_i' and 'b_j' with the output image being '$T^k(b_i, b_j)$'. Finally, encryption 'E' is performed by combining the PR '$T^k(b_i, b_j)$' and updated '$\Delta W_{ij}(p)$' forming modulus of number of neurons 'l' as expressed below.

$$E = \big[T^k(b_i, b_j) + \Delta W_{ij}(p)\big]\, mod\, l \quad (13)$$

Fig. 6 given below shows the resultant images after compression/decompression.

The pseudo code representation of poincare recurrence network lossless compression is given below.

Algorithm 2 Poincare recurrence network lossless compression

Input: Dimensionality reduced images '$DRI = d_1, d_2, \ldots, d_n$', learning factor '$\mu$'
Output: PSNR improved lossless compression
Step 1: **Initialize** band size '$n * n$', vector size 'm', pixels 'N' Step 2: **Begin** Step 3: **For** each dimensionality reduced images 'DRI' Step 4: **For** each band 'b' //compression Step 5: Measure random weight using equation (7) Step 6: Obtain hidden layer using equation (8) Step 7: Evaluate output layer using equation (9) Step 8: Update the weights using equation (10) Step 9: Measure error gradient using equation (11) Step 10: Evaluate Point Care Recurrence using equation (12) Step 11: Perform encryption with equation (13) Step 12: Return (compressed image '$CDRI$') Step 13: **End for** Step 14: **End for** Step 15: **End**

Table 1. Light field images storage of GDW-PRN, existing C-DPCM [1] and 3DWT-SRV [2]

Samples	**Light field images storage (KB)**		
	GDW-PRN	C-DPCM [1]	3DWT-SRV [2]
15	30	45	60
30	60	90	120
45	90	100	140
60	120	135	160
75	140	160	190
90	180	190	210
105	210	230	250
120	230	280	310
135	250	300	340
150	290	340	390

The poincare recurrence network lossless compression algorithm initialises bands with respect to each vector to obtain random weight for each dimensionality reduced image input.

4. Experimental settings

This section analyses recreation results to

evaluate greedy discrete wavelet and poincare recurrence network (GDW-PRN) for robust lossless image compression of hyper spectral images. Our experiments made use of a database obtained from the SPECIM hyperspectral image repository, which covers the 900 - 1700 nm spectral range and is extensively utilised in industrial quality control. [21]. To compare two methods, compression outcomes based on differential-pulse-code-modulation [1] method and outcomes of 3D wavelet transform and spectrum learning with regression vector (3DWT-SRV) [2], the same images are used. Light field image storage and peak S/N ratio evaluate the proposed method.

4.1 Performance measure of light field images storage

A significant amount of storage is said to be incurred during lossless image compression/ decompression with respect to light field images storage. The light field images storage is mathematically expressed as given below.

$$LFIS = \sum_{i=1}^{n} S_i \; MEM \; (Comp/Decomp) \quad (14)$$

From Eq. (14), light field images storage "LFIS" is measured by the samples provided as input "S i" and the memory consumed in compression or decompression "MEM (Comp/Decomp)" denoted by KB-worthy. Table 1 shows how GDW-PRN, C-DPCM, and 3DWT-SRV compressed 150 samples at different values to store light field images. Compared to [1] and [2], proposed GDW-PRN stores light field images of reconstructed images better.

Fig. 7 shows light field image compression/ decompression storage. 15–150 hyper spectral images of various sizes were examined. Samples increase compression rate and light field image storage. GDW-PRN consumed 30KB, [1] 45 KB, and [2] 60 KB in simulations for 15 samples with different image sizes. GDW-PRN reduces light field image storage by 16% over [1, 2].

4.2 Performance measure of PSNR

Peak S/N ratio refers to the ratio of the original hyperspectral image and the distorted images. The Peak S/N ratio is measured as follows,

$$PSNR = 10 \; log_{10} \left[\frac{S^2}{MSE} \right] \quad (15)$$

$$MSE = \left(S - S' \right)^2 \quad (16)$$

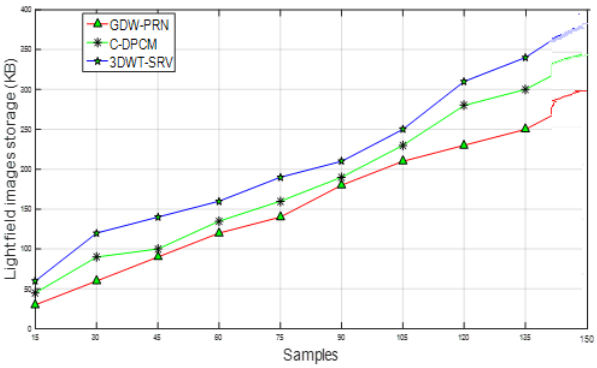

Fig. 7 Graphical representation of light field images storage

Table 2. PSNR of GDW-PRN, existing C-DPCM [1] and 3DWT-SRV [2]

Samples	PSNR (dB)		
	GDW-PRN	C-DPCM [1]	3DWT-SRV [1]
15	39.04	37.3	35.85
30	41.35	38.35	36.15
45	42.55	39.55	37
60	43.15	40.15	38.35
75	45.55	41.35	39
90	46	42	40.25
105	46.15	44.55	40.35
120	46.85	45.35	41
135	47	45.85	42.45
150	47.35	46	43

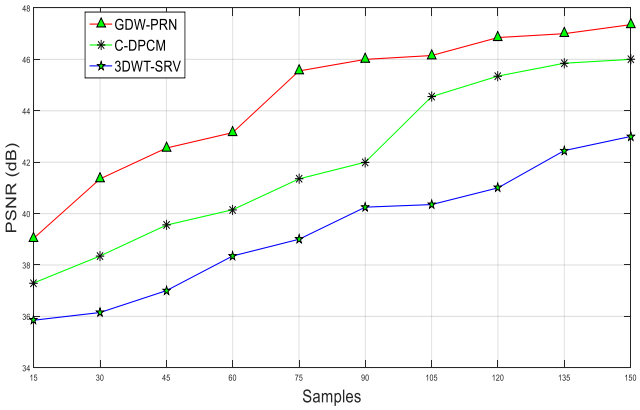

Figure. 8 Graphical representation of PSNR

From Eqs. (15) and (16), the peak S/N ratio is the log value of the possible pixel value of the hyperspectral sample image "S" and the mean

square error-MSE. Mean Square Error-MSE is the square variance between the original hyperspectral sample image "S" and noisy image "S^". The maximum pixel value is dB. Table 2 shows PSNR for hyper spectral images.

Fig. 8 depicts PSNR with 150 samples. Peak S/N ratio, which affects characterization accuracy, is the ratio between the maximum possibility of a single and corrupting noise. It is widely used to assess lossless compression image restoration quality.

The figure suggests that GDW-PRN improves PSNR. In other words, from the simulations with 25 samples, the mean square error "MSE" using GDW-PRN was 81dB, C-DPCM was 121dB [1] and 169dB [2]. With this MSE value, the C-DPCM returned 39.04 dB, 37.30 dB, and 35.85 dB PSNR values [1, 2]. GDW-PRN had a higher PSNR than [1] and [2] based on simulation results. Greedy Band dimensionality-reduced visual data representation caused this. This Greedy Band measured two independent bands using proximity. GDW-PSNR PRN's was 6% and 7% better than [1] and [2].

In continuation to the performance evaluation compared for three parameters such as Light field images storage (KB) and peak signal to noise ratio (PSNR), the investigation has been extended for other quality metrics such as normalized cross-correlation (NC), structural content (SC), and normalized absolute error (NAE) and are provided in Table 4. For the purpose of further investigation, the sample image considered was sample 2. The derived quality metrics for the sample 2 is provided in Table 3. The quality metrics NAE, SC and NCC are plotted in Fig. 9. Physical quality metric links the compressed image's mass to the unique image's weight globally.

A small average value discrepancy indicates excellent image quality. This parameter is close to 1, so the method works. –1 to 1 is NCC. Values may drop over unity. Correlation coefficients of –1 and above 1 indicate perfect correlation and anti-correlation.

5. Conclusion

Hyperspectral image lossless compression/ decompression using discrete wavelet greedy band and Poincare recurrence network is proposed. Wavelet reduction with sub sampling eliminates noise and improves decoding quality, providing a good simple band for visual data representation. Greedy band function reduces pre-processed hyper spectral image dimensions. Since each band is estimated by the affinity in the adjacent band,

Table 3. Quality metrics derived for sample 2

Sample	Quality Metrics	Values
Sample 2	Normalized Cross-correlation (NC)	1.0792
	Structural Content (SC)	0.8552
	and Normalized Absolute Error (NAE)	0.1004

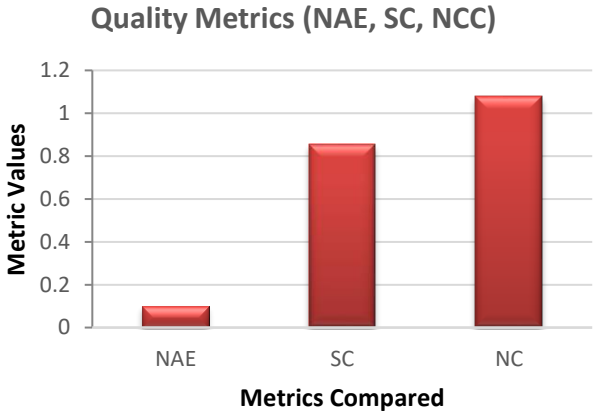

Figure. 9 Quality metrics NAE, SC, NCC

greedy proximity detection reduces dimensionality. Finally, poincare recurrence theorem compresses/decompresses. Experimental results show that the algorithm compresses hyperspectral images by improving PSNR and light field image storage. The mean square error using the proposed GDW-PRN was 81dB, which is less than the MSE of two other methods, indicating that the proposed work is better and the PSNR is automatically good. The algorithm also provided effective results for NAE, NCC and SC for a sample image.

Conflicts of interest (Mandatory)

The authors declare that they have no known competing financial interests or personal relationships that could have appeared to influence the work reported in this paper.

Author contributions

Anjaneya.P: Conceptualization, Data curation Formal analysis, Methodology, Software Writing, original draft, investigation, resources. Rajini G.K: Writing—review and editing, visualization, supervision, project administration.

References

[1] J. Luo, J. Wu, S. Zhao, L. Wang, and T. Xu, "Lossless compression for hyperspectral image using deep recurrent neural networks",

International Journal of Machine Learning and Cybernetics, Vol. 10, pp. 2619-2629, 2019.

[2] N. Zikiou, M. Lahdir, and D. Helbert, "Support Vector Regression-Based 3D-Wavelet Texture Learning for Hyperspectral Image Compression", *The Visual Computer*, Vol. 36, No. 7, pp. 1473-1490, 2019.

[3] Y. Tian, H. Zeng, J. Hou, J. Chen, and K. Ma, "Light Field Image Quality Assessment via the Light Field Coherence," *IEEE Transactions on Image Processing*, Vol. 29, pp. 7945–7956, 2020.

[4] G. Wu, B. Masia, A. Jarabo, Y. Zhang, L. Wang, Q. Dai, T. Chai, and Y. Liu, "Light Field Image Processing: An Overview", *IEEE Journal of Selected Topics in Signal Processing*, Vol. 11, No. 7, pp. 926-954 , 2017.

[5] S. S. Tamboli, V. R. Udupi, and B. N. Subudhi, "An efficient framework for increasing image quality using DRN Bi-layer enfolded compressor", *Multimedia Tools and Applications*, Vol. 79, pp. 12401–12426, 2020.

[6] G. Kiranmaye and S.Tadisetty, "A novel ortho normalized multi-stage discrete fast Stockwell transform based memory-aware high-speed VLSI implementation for image compression", *Multimedia Tools and Applications*, Vol. 78, pp. 17673–17699, 2019.

[7] J. Li, Z. Liu, and S. Tian, "An efficient onboard compression method for multispectral images using distributed post-transform in the wavelet domain in conjunction with a fast spectral decorrelator", *Optical Review*, Vol. 26, pp. 247–261, 2019.

[8] S. Karimullah and D. V. Vardhan, "Pin density technique for congestion estimation and reduction of optimized design during placement and routing", *Applied Nanoscience*, Vol. 13, No. 3, pp. 1819-1828, 2022.

[9] J. Uthayakumar, T. Vengattaraman, and P. Dhavachelvan, "A survey on data compression techniques: From the perspective of data quality, coding schemes, data type and applications", *Journal of King Saud University – Computer and Information Sciences*, Vol. 33, No. 2, pp. 119-140, 2018.

[10] R. Birman, Y. Segal, and O. Hadar, "Overview of Research in the field of Video Compression using Deep Neural Networks", *Multimedia Tools and Applications*, Vol. 79, No-. 17-18, pp. 11699–11722, 2020.

[11] S. Karimullah and D. V. Vardhan, "Iterative Analysis of Optimization Algorithms for Placement and Routing in Asic Design", In: *Proc. of ICDSMLA, 2019, Lecture Notes in Electrical Engineering, Springer Nature Singapore Pte Ltd*. Vol. 601, 2020.

[12] E. Magli, M. Mancin, and L. Merello, "Low-complexity video compression for wireless sensor networks", In: *Proc in International Conference on Multimedia and Expo.*, Vol. 3, No. 9, pp. 585-588, 2003.

[13] H. Zaineldin, M. A. Elhosseini, and H. A. Ali, "Image compression algorithms in wireless multimedia sensor networks: A survey", *Ain Shams Engineering Journal*, Vol. 5, No. 4, pp. 1411-1422, 2014.

[14] R. Kumar, and U. P. Kumar, "An efficient technique for image compression and quality retrieval using matrix completion", *Journal of King Saud University – Computer and Information Sciences*, Vol. 31, No. 8, pp. 991-998, 2019.

[15] L. Wang, J. Bai, J. Wu, and G. Jeon, "Hyperspectral Image Compression based on Lapped Transform and Tucker Decomposition", *Signal Processing-Image Communication*, Vol. 36, pp. 63-69, 2015.

[16] D. Valsesia and E. Magli, "High-Throughput Onboard Hyperspectral Image Compression with Ground-Based CNN Reconstruction", *IEEE Transactions on Geoscience and Remote Sensing*, Vol. 57, No. 7, pp. 4789-4802, 2019.

[17] T. Bruylants, A. Munteanu, and P. Schelkens, "Wavelet Based Volumetric Medical Image Compression", *Signal Processing: Image Communication*, Vol. 31, pp. 112-133, 2015.

[18] C. Yang, X. Zhang, C. Zhong, C. Liu, J. Pei, K. R. Mohanarao, and J. Chen, "A spatiotemporal compression based approach for efficient big data processing on Cloud", *Journal of Computer and System Sciences*, Vol. 80, pp. 1563-1583, 2014.

[19] Y. Nian, M. He, and J. Wan, "Distributed near lossless compression algorithm for hyperspectral images", *Computers and Electrical Engineering*, Vol. 40, No. 3, pp. 1006-1014, 2014.

[20] N. R. M. Noor and T. Vladimirova, "Investigation into lossless hyperspectral image compression for satellite remote sensing", *International Journal of Remote Sensing*, Vol. 34, No. 14, pp. 5072–5104, 2013.

[21] https://www.specim.com/library/